Light & Engineering
Vol. 28, No. 4, pp. 103–110, 2020

https://doi.org/10.33383/2019-012
Svetotekhnika #3, 2020, pp. 71–77

A COST-EFFECTIVE ILLUMINANCE SENSOR FOR DAYLIGHT-HARVESTING LIGHTING CONTROL SYSTEMS

Moutusi Bag, Saswati Mazumdar, and Kalyan Kumar Ray

Jadavpur University, Kolkata, India
E-mails: bag12moutusi@gmail.com,
saswati.mazumdar@gmail.com,
kalyancs.ray@gmail.com

ABSTRACT

A cost-effective two-wire industrial standard illuminance sensor (4–20) mA has been proposed. It can be used for daylight harvesting control of indoor illuminance and other applications. The basic sensor used is a cadmium sulphide (*CdS*) light dependent resistor, whose relative spectral characteristic almost corresponds to the human eye. The method of sensor calibration has been presented and static and dynamic performance characteristics of the sensor have been experimentally determined.

Keywords: daylight-harvesting, relative spectral response, light dependent resistor (LDR), silicon *PIN* photodiode, current controlled current sink, infrared-cut filters, static performance, dynamic performance, points-of-control

1. INTRODUCTION

1.1. General Background

Two-wire sensors have been very popular in measurement of commonly encountered process variables like temperature, pressure, traffic flow, level of illuminance, etc. [1–4]. The most important reasons for their popularity are the absence of any auxiliary power supply, low cost of wiring and simplicity of installation. The necessity of using a two-wire sensor for illuminance measurement was felt during the development of a daylight-harvesting lighting scheme, in which natural daylight supplements artificial dimmable light emitting diode (LED) luminaires to provide a highly energy-efficient lighting system [5–9], [20–21]. As commercially available sensors for the purpose were either not easily available or were costly, it was necessary to develop one with a high performance/cost ratio. A large number of sensors (typically 1 to 4 per thousand m^2) may be required to maintain a uniformity of illuminance. This makes the cost of the sensor and the wiring cost very important factors in the design.

1.2. LDR as an Illuminance Sensor

Our initial attempt to develop a cost-effective indirect illuminance measurement system for daylight harvesting applications was biased towards using a silicon *PIN* photodiode (SIPD) as the basic sensing element. The obvious fact of high linearity of the short-circuit photocurrent as a function of the incident illuminance LED to this bias [13]. However, several disadvantages of this sensor were apparent during the development process. Firstly, the amplifier needed to amplify the photocurrent to the level of usable current or voltage required a bipolar power supply, which required two supply wires (apart from the ground). Another approach was to use an on-board positive-to-negative voltage converter, causing increase of complexity, cost and supply current requirements. A supply current more than 4 mA implied that an industry-standard 2-wire (4–20) mA signal output could not be produced. This

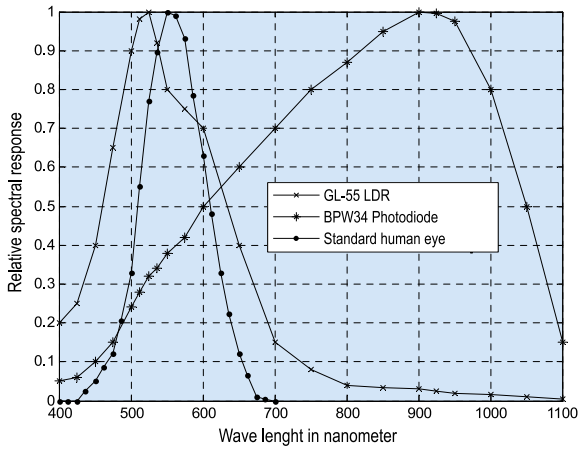

Fig. 1. Relative spectral response characteristics of a typical *Si PIN BPW 34* photodiode, a LDR and standard human eye

meant that one has to remain satisfied output of (0–10) V or (0–5) V with all associated demerits of a voltage-type sensor [3]. It would take four or at least three wires to connect such a sensor to a remote instrument or controller.

The second factor, which made an SIPD not very amenable to our application, was a great mismatch between its spectral response and the response of the human eye. The relative spectral response characteristic of a typical SIPD is shown in Fig. 1. An average human eye responds to wavelengths from 360 nm to 720 nm and has a peak of response of about 555 nm. The 10 % of the peak response occurs at about 425 nm and 675 nm. As shown in Fig. 1, 10 % of the peak response of an SIPD extends wide into the infrared region, up to about 1080 nm, thereby making it quite sensitive for wavelengths above the visible spectrum. Unless it is used along with a proper infrared-stop optical filter, an SIPD produces a higher output for a source containing infrared light (e.g. daylight or incandescent source) than one, which does not contain it (e.g. white LED or fluorescent lamp), while same produces the same illuminance in the visible range. Since the required infrared-cut filters were expensive and not very available, the research in this direction was abandoned. A photodiode with an integral optical filter was announced, which has a spectral response almost corresponding to the human eye, as *TEMT6200FX01* [14]. Issues of availability and cost kept us from using it in this study.

The peak spectral response of human eye for photopic vision occurs at 555 nm. The relative spectral responses (RSR) of a *CdS* LDR and a Si PIN photodiode are shown in Fig. 1. The RSR of common *CdS* LDRs [15–16] has a spectral peak at 525 nm. In addition, at 800 nm, which is above the visible range, the RSR falls only to 0.04. In contrast, a *PIN* diode sensor has an RSR of 0.87, which is completely unacceptable.

The basic equation representing the variation of the terminal resistance *R (E)* depending on the incident illuminance *E* is given in [16]

$$R\left(E\right)\cdot E^{\gamma} = K, \tag{1}$$

where γ is a constant known as illuminance index of the LDR and *K* is a constant.

Considering two illuminances E_1 and E_2 the following can be obtained

$$R\left(E_1\right) \,/\, R\left(E_2\right) = \left(E_2 \,/\, E_1\right)^{\gamma}. \tag{2}$$

Manufacturers determine the value of γ based on two measurements at E_1 = 10 lx and E_2 = 100 lx. Thus, we get

$$R\left(10\right) \,/\, R\left(100\right) = 10^{\gamma} \quad \text{or} \quad \gamma = lg\frac{R\left(10\right)}{R\left(100\right)}. \tag{3}$$

Section 3 describes an experimental method for evaluation of an approximate value of γ.

2. PRINCIPLE OF OPERATION OF THE SENSOR

2.1. Block Diagram Description

The principle of operation can be understood by considering the cascade combination of three blocks, as shown in Fig. 2. The first block converts the incident illuminance *E* into a low-level voltage u_1 with a typical full-scale value of 90 mV. This voltage is amplified to a higher-level u_2 using an amplifier *A*1. A typical full-scale value of u_2 is about 1 V. To improve the linearity of the transmitter at low values of *E*, a fixed offset is also added to the output.

The second block generates two currents i_{21} and i_{22} using two 2-terminal components marked as *VIC*1 and *VIC*2. *VIC*1 is actually a variable linear resistor. *VIC*2, on the other hand, is a non-linear resistor, as discussed in section 2.2. The *VIC*s are se-

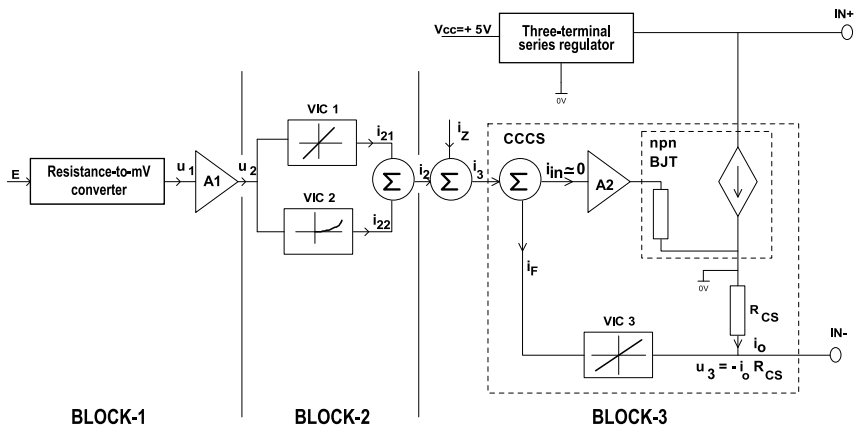

Fig. 2. Simplified block diagram of the sensor

lected in such a way that the sum i_2 of the two-component currents i_{21} and i_{22} is a linear function of the illuminance E.

The third block takes the sum of i_2 and adjustable current i_z to produce the current i_3. The current i_3 is then fed to the current controlled current sink (CCCS), so that the current i_o drawn between the transmitter terminals *IN+* and *IN-* is an amplified replica of i_3. This block utilizes an op-amp and a medium-power *NPN* bipolar junction transistor (BJT). A detailed explanation is given at the end of this section.

An expression for the output current i_o may be considered now. Clearly, i_o is given by

$$i_o = G_i \cdot (i_2 + i_z), \tag{4}$$

where G_i is the gain of the CCCS.

Since i_2 is proportional to E, Eq. 4 is modified to

$$i_o = K_1 \cdot E + K_2, \tag{5}$$

where K_1 is a constant and $K_2 = G_i \cdot i_z$ is also a constant. For an ideal transmitter K_2 caters for the "live-zero" component of the output current, which is commonly 4 mA.

2.2. Circuit Realization of the Functional Blocks

The circuit diagram of the first block is shown in Fig. 3. The photocurrent of the LDR, which is a function of incident illuminance E, flows through the variable resistor $R1$ and produces the input voltage u_1 of the amplifier [17]. The resistor $R1$ should have a value small in comparison with the resistance of the LDR at the full-scale value of E. For the supply voltage Vcc = 5 V the value of u_1 is kept within 90 mV at full scale. This ensures that the terminal voltage across the LDR is nearly constant.

The amplifier uses one-half of a common *LM358* operational amplifier in a non-inverting configuration in [17] and [18]. If there is no resistor $R4$, the gain of the amplifier $G_v = u_2 / u_1$ is set by

$$G_v = 1 + R2 / R3, \tag{6}$$

where $R2$, $R3$, and $R4$ are appropriate resistors on the circuit in Fig. 3.

However if $R4$ is present in the schema the expression for u_2 is modified as follows:

$$u_2 = (1 + R2 / R3) \cdot u_1 - (R2 / R4) \cdot V_{cc}.$$

The above expression reduces to the following

$$u_2 = G_v \cdot u_1 + u_{20}, \tag{7}$$

where

$$u_{20} = -(R2 / R4) \cdot V_{cc}. \tag{8}$$

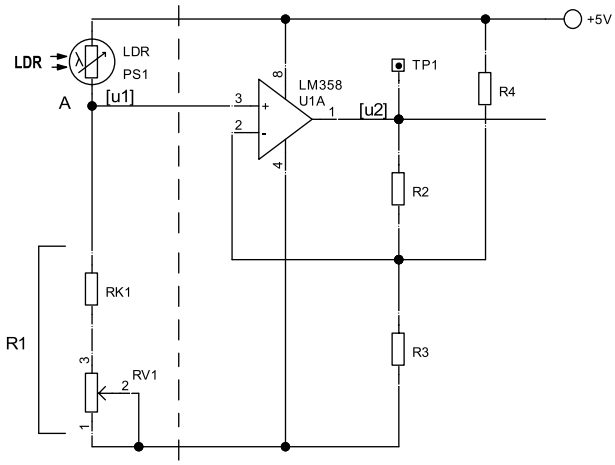

Fig. 3. Illuminance to voltage converter and linear amplifier

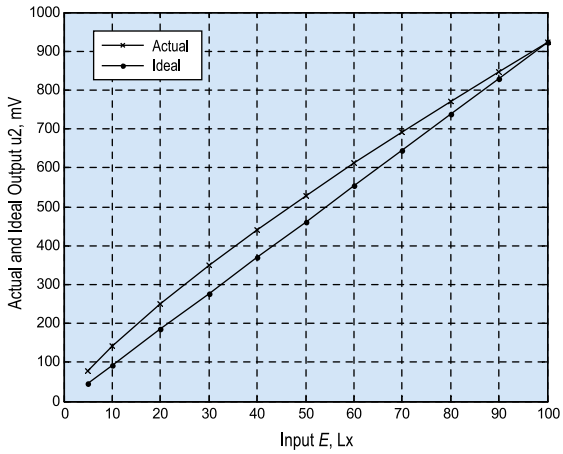

Fig. 4. Amplifier 1 output as a function of incident illuminance *E*

In our study, we have used values of *R*2 and *R*3 as 10 K and 1 K, respectively, so as to get a G_v of 11. A fixed *R*4 value of 1 MΩ produced a fixed output offset of 5 mV, which was good enough for all transmitters. The value of *RV*1 the variable part of *R*1 was adjusted so that at 40 % of E_{FS}, the full scale value of *E*, the value of the output u_2 becomes 440 mV.

For a typical LDR with a γ = 0.81 and *R* (100) = 7.1 KΩ, the variation of u_2 as a function of *E* is shown in Fig. 4. It may be observed here that the function is nonlinear. The maximum deviation of about 72 mV occurs at 40 % of span. The slope of *E* (u_2) graph is a monotone decreasing function of *E*. The latter observation is true irrespective of the values of γ and *R* (100).

The circuit realization of the second block is shown in Fig. 5. The ground terminal shown on the right side of this figure attains a potential very close to ground due to reasons explained in the next section. Thus, the current in the upper branch i_{21} is set as follows:

$$i_{21} = u_2 / R5 \quad , \tag{9}$$

where *R*5 is a variable resistance consisting of a series combination of series resistance of *RK*5 and *RV*5. Thus, the value of i_{21} corresponding to any u_2 can be adjusted using *RV*5. Graph i_{21} as a function of *E*, by virtue of Eq. 9, has the same form as Fig. 4. Since $\frac{du2}{dE}$ is a monotonically decreasing function of *E* and $i_{21} = u_2/R5$, the same nature is found in the function i_{21} (*E*). The voltage to current converter *VIC*2 produces a complementary non-linearity,

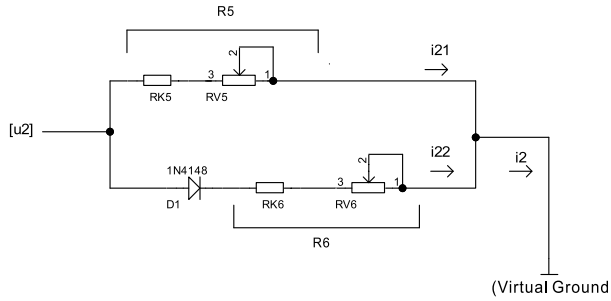

Fig. 5. Amplifier output to linear and non-linear current converter

whose slope is monotone increasing in nature. The character of the latter complementary function i_2 should be such that the sum of the component currents i_{21} and i_{22} becomes a linear function of *E* over the operating range.

Assuming that *D*1 to be an ideal diode with a fixed threshold voltage V_F and a negligible dynamic resistance, i_{22} is given as follows:

$$i_{22} = 0, \; if \; u_2 < V_F,$$

$$i_{22} = (u_2 - V_F)/R6, \; if \; u_2 \geq V_F, \tag{10}$$

where *R*6 consists of a fixed part of *RK*6 and a variable part of *RV*6 sequentially.

It is easy to graph the characteristics of u_2 (i_{22}) given by Eq. 10. It will have a zero slope until the voltage reaches the value of V_F and a slope of 1/*R*6 for higher voltages. Such an abrupt change in slope is not observed when using a physical low-signal diode e.g. *1N4148* is used. The u_2 (i_{22}) graphs for three different *R*6 values, namely 8.2 KΩ, 10 KΩ, 12 KΩ, in series with the *1N4148* are shown in Fig. 6. It is observed that for a fixed u_2, the current i_{22} reduces with increasing *R*6, and for a fixed *R*6 the slope of the graph monotonically increases with increasing u_2.

The circuit realization of the third block is now considered. The output stage of the sensor that works as a current-controlled current sink [19] is shown in Fig. 7. Of the two output terminals marked *I*+ and *I*-, the former is connected to the positive side of the loop supply of (8–24) V range, and the latter is connected to the ground side of the same supply via a current sensing resistor R_{cs} (not shown in the figure). The drop across R_{cs} is used to measure the current output of the sensor. The path of the output current I_o is shown by thick lines in the same figure. Due to the flow of I_o, a voltage u_3 is generated across *R*14

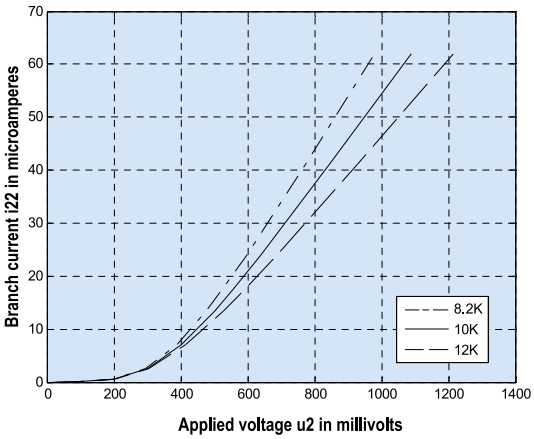

Fig. 6. i_{22} as function of u_2 for various values of $R6$

$$u_3 = -i_o \cdot R14. \tag{11}$$

This consequently produces a current i_F in the indicated direction given by

$$i_F = u_3 / R13. \tag{12}$$

Combination of Eq. 11 and Eq. 12 gives

$$I_O = i_F \cdot G_I, \tag{13}$$

where G_I is the current gain factor given by

$$G_I = R13 / R14. \tag{14}$$

The required expression of the output current as a function of the currents i_2 and i_Z can be obtained by considering the *Kirchhoff's* current equation at node *B*, which is

$$I_2 + i_Z = i_F,$$

since the input current I_{in} at the non-inverting input of the opamp *U*1 can be neglected in comparison with other terms. Substitution of i_F from Eq. 13 and the fact that

$$i_Z = V_{cc} / R7, \tag{15}$$

therefore, yields that

$$i_O = G_I \cdot \left(i_2 + V_{cc} / R7\right). \tag{16}$$

Eq. 16 indicates that at zero illuminance (E = 0), since both i_{21} and i_{22} have zero values, i_2 has a zero value and the output current assumes a value of V_{cc} / *R*7, which can be adjusted to its nominal value of 4 mA by adjustment the variable part of *R*7, namely

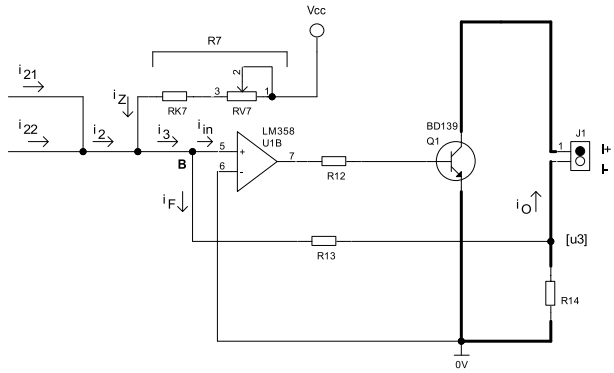

Fig. 7. Current summer and output current converter

*RV*7. As will be seen later, this will form a step in the calibration procedure of the sensor.

3. APPROXIMATE DETERMINATION OF γ AND SELECTION OF A SUITABLE LDR

Under the condition, that the voltage u_1 is very small compared to *Vcc*. The values of u_1 at 10 lx and 100 lx are given by

$$u_1(10) \approx \frac{Vcc}{R(10)} R_1, \tag{17}$$

$$u_1(100) \approx \frac{Vcc}{R(100)} R_1. \tag{18}$$

Division of Eq. 18 by Eq. 17 yields

$$\frac{u_1(100)}{u_1(10)} \approx \frac{R\ (10)}{R\ (100)}\ . \tag{19}$$

In the absence of the output offset voltage u_{20}, which can be ensured by omitting *R*4 in Fig. 3, the left side of Eq. 19 can be replaced by u_2 (100) / u_2 (10), since u_1 and u_2 are related by a constant gain factor *Gv*. Thus,

$$\frac{u_2(100)}{u_2(10)} \approx \frac{R\ (10)}{R\ (100)}\ . \tag{20}$$

A combination of Eq. 20 with Eq. 3 therefore produces

$$\gamma \approx lg\ \frac{u_2(100)}{u_2(10)}. \tag{21}$$

Eq. 21 gives us a convenient way of determining the approximate γ. Our experience shows that if the approximate γ lies in the range (0.7–0.85), the resulting sensor can give a linearity of better than 1 %. Thus, an LDR with the measured γ outside the range was rejected.

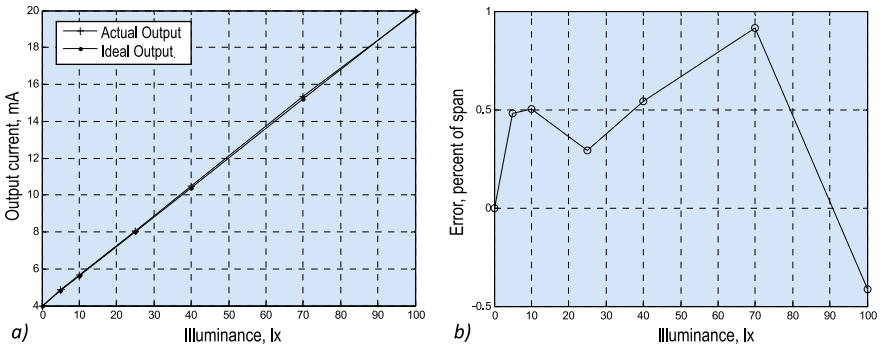

Fig. 8. Actual and ideal output characteristics (a) and graph of the sensor error (b)

4. CALIBRATION OF THE SENSOR

To calibrate the sensor, the sensor head was placed in close proximity of a calibrated illuminance meter placed in a light tight box. A white LED light source was placed above the sensor, and the current values of the LED were selected so that when two switches with appropriate marking were turned on, it was possible to obtain illuminances of 40 lx and 100 lx. Turning off both switches creates a zero illuminance condition on the sensor. The *IN*+ and *IN*- terminals of the sensor are connected to a 12 V DC power supply via a milliammeter. The following steps are then executed to calibrate the sensor.

1. Create 0 lx condition. Adjust *RV*7 (Fig. 7) so that i_O = 4 mA.

2. Keep *RV*6 at its maximum value.

3. Set *E* = 100 lx and adjust *RV*5 (Fig. 5) so that i_O becomes 90 % of its full scale value, i.e. 18 mA.

4. Set *E* = 40 lx and adjust *RV*6 (Fig. 5) so that i_O becomes (4+0.4·16), i.e. 10.4 mA.

5. Set *E* = 100 lx and adjust *RV*5 (Fig. 5) so that i_O becomes 20 mA.

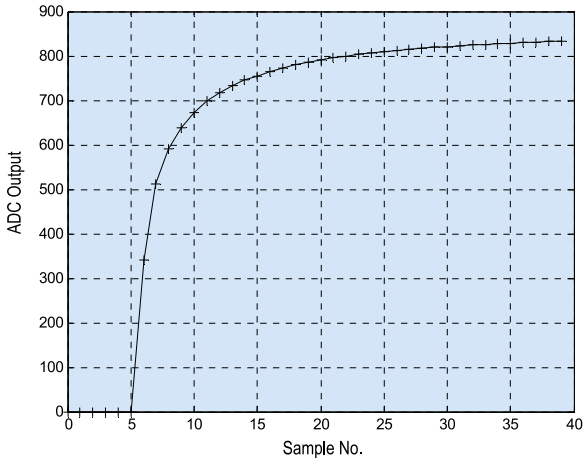

Fig. 9. Step response of the sensor

Repeat steps (4) and (5) until the sensor is calibrated at both 40 lx and 100 lx.

The performance of the sensor over the entire range of (0–100) lx is described in the next section.

5. EXPERIMENTAL RESULTS

The results given in this section have been obtained for a sensor using an LDR with an approximate γ of 0.78, as determined by the method in section 3.

5.1. Static Performance

The ideal and actual output currents of the sensor are shown in Fig. 8.(a), where the measured values correspond to *E* = 0 lx, 5 lx, 10 lx, 25 lx, 40 lx, 70 lx, and 100 lx. The error is so small that it is impossible to accurately measure with the help of the graph. The graph of the function *Error (E)* is therefore presented in Fig. 8.(b). It is observed that the maximum error magnitude is less than 1 % of the span of 16 mA.

5.2. Dynamic Performance

An experiment was performed to evaluate the time constant of the first-order model of the sensor. The terminal current is made to pass through a 100 Ω resistor. The resulting voltage drop is converted to a number using a 10 bit A-to-D converter. A step increment in *E* from 0 lx to 100 lx is applied, and the resulting output of the ADC is stored for 800 ms at 20 ms intervals. A graph of the stored values is shown in Fig. 9 where the step in *E* has been applied at 100 ms. Observing that the steady state ADC output is about 840, the time constant of the sensor is approximately 40 ms, which is equal to the time taken to reach 0.632 times the steady-state value.

Fig. 10. Photo of the typical wall mounted sensor

6. CONCLUSION

6.1. Hardware Variants of the Sensor

Two different hardware variants of the sensor were built using the LDR sensor and its associated circuit. The first one is wall-mounted, and the second one is for ceiling mounting. A photo of the wall-mounted version is shown in Fig. 10. The sensor head is placed at the back of the cylinder with a diameter of 25 mm and length of 30 mm. The cylinder makes an angle of 45° with a matte-white horizontal platform. The incident light on the platform which, is the result of different light sources in a room, generates the light incident on the sensor. In a typical lighting control system, the output variable from several sensors can be combined to calculate the illuminances at several points of interests in the room.

Another version of the sensor, meant for ceiling mounting, has a simpler construction. The LDR is placed behind a cylinder with a diameter of 20 mm and a length of 20 mm long, the open end of which faces the floor. The results in a conical zone with a total viewing angle of about 53 °. The output of such a sensor is a function of the illuminance on the work surface is included in the viewing area.

6.2. Applications

The sensor described in this study can be used in applications where the primary requirements are low cost, two-wire connection, and indirect placement (on wall or ceiling) [11]. In addition, since the self-low cost components have been used, the system specification costs are very low compared to commercially available sensors. The latter requirement is based on the fact that in most cases the required sensor can not be installed directly on the work surface.

In our study, this type of sensor is used in an integrated feedback lighting system where daylight is used to supplement artificial dimmable luminaires based on LED. This concept of daylight harvesting control gives significant savings in electrical energy and uniformity of illuminance at preselected points-of-control (POC) on the work surface [10, 12]. In the present scheme, there are six ceiling-mounted LED luminaires and four wall-mounted sensors in a (6.2 m × 4.1 m) room with windows on one side. There are 6 POCs where the illuminances due to the combined contributions of artificial lighting and daylighting are to be maintained at set-point values. The illuminance data available from the four sensors are converted into the six illuminances at the POCs by using a suitable matrix transformation.

REFERENCES:

1. Bela G. Liptak. Instrument Engineers Handbook. Boca Raton, London, New York, Washington: D.C., CRC Press, 4th Edition, 2003.

2. John G. Webstar. The Measurement, Instrumentation And Sensors Hand book. N.W., Boca Raton: CRC Press, and IEEE Press, 1999.

3. Carlos A. dos Reis Filho, An integrated 4–20 mA two-wire transmitter with intrinsic temperatures sensing capability, IEEE Trans. Solid-State Circuits, Aug., 1989. V24, #4, pp. 1136–1142.

4. Murata Power Solutions, DMS Application Note 20: 4–20 mA Current Loop Primes. [Online]. Available: www.murata-ps.com/support.

5. Li S., Pandharipande A. Daylight sensing LED lighting system, IEEE sensors journal, May 1, 2016. V16, #9, pp. 3216–3223.

6. Pandharipande A., Li S. Light-harvesting wireless sensors for indoor lighting control, IEEE sensor journal, December, 2013. V13, #12, pp. 4599–4606.

7. Pandharipande A., Caicedo D., Smart indoor lighting systems with luminaire-based sensing: A review of lighting control approaches, Energy Buildings (Oct. 2015). V104, pp. 369–377.

8. D. Caicedo, A. Pandharipande, F. M.J. Willems, Light sensor calibration and dimming sequence design in distributed lighting control systems, Proc. IEEE11th Int. Conf. Netw. Sens. Control (ICNSC), Apr. 2014. pp. 344–349.

9. D. Caicedo, A. Pandharipande, F. M.J. Willems, Illumination gain estimation and tracking in a distributed lighting control system, Proc. IEEE Multi-Conf. Syst. Control (MSC), Oct. 2014. pp 1650–1655.

10. A. Pandharipande, S. Li, Illumination and light sensing for daylight adaptation with an LED array: Proof-of-principle, Proc. 39th Annu. Conf. IEEE Ind. Electron. Soc. (IECON), Nov., 2013. pp. 6081–6086.

11. P. Dietz, W. Yerazunis, D. Leigh, Very low-cost sensing and communication using bidirectional LEDs, Proc. 5th Int. Conf. Ubiquitous Comput, Oct., 2003. pp. 175–191.

12. M. G. Villalva, J.R. Gazoli, E.R. Filho, Modeling and circuit-based simulation of photovoltaic arrays, Proc. Power Electron. Conf. (COBEP), 2009. pp. 1244–1254.

13. BPW34 datasheet, Vishay Semiconductors. [Online]. vailable: www.vishay.com/doc?91000.PDF

14. TEMT6200FX01 datasheet, Vishay Semiconductors.[Online]. Available: www.vishay.com/doc?91000.

15. Plastic coated CdS photocells. [Online]. Available: www.selcoproducts.com

16. PGM CDS Photo resisters, version 2010. [Online]. Available: www.token.com/tw

17. A. S. Sedra and K.C. Smith, Microelectronic Circuit, New York: Oxford University press, 1998.

18. Sergio Franco, Design with operational amplifiers and analog integrated circuits. NY, USA: McGraw-Hill Education, 2015.

19. Toumazou, C., Lidgey, F. J. and Haigh, D. G., (EDS), Analogue IC design: the current-mode approach. London: IEE, Peter Peregrinus Ltd, April 1990.

20. GaspareBoscarino, MehrdadMoallem, Daylighting control and simulation for LED-based energy-efficient lighting systems, IEEE transsactions on industrial informatics, February 2016. V12, #1, pp. 301–308.

21. Karl W. Boer, Cadmium sulfide enhances solar cell efficiency, Energy conversion and management, Elsevier, 2011. #52, pp. 426–430.

Moutusi Bag

received her M. Sc. degree in Instrumentation and Control Engineering from University of Calcutta, India in 2010. She is currently pursuing Ph.D. in Engineering at Jadavpur University, India. Her research interests are in the area of daylight harvesting for indoor lighting control and solar based lighting system

Kalyan Kumar Ray

received the B. Sc. degree from Jadavpur University, Kolkata, India, in 1968, where he was adjudged the best student in the Faculty of Engineering and Technology, the M. Sc. degree from the Indian Institute of Technology, Kanpur, India, in 1970, and the Ph.D. degree from Jadavpur University in 1979, all in electrical engineering. He was a Senior Research Assistant in the Indian Institute of Technology, Kanpur, from 1968 to 1973. In 1973, he joined Jadavpur University, Kolkata, India, as a Lecturer. He served in the Departments of Electrical Engineering and Instrumentation and Electronics Engineering for 39 years and retired as a Professor. He was Principal Investigator in several Government-funded projects. He is currently a Consultant to industries manufacturing electronic systems. His primary research interests include control of power electronic converters, embedded control and instrumentation, solar photovoltaic conversion, and vehicular electronics

Saswati Mazumdar

received the B. Sc., M. Sc., and Ph.D. degrees in electrical engineering (EE) from Jadavpur University (JU), Kolkata, India, in 1982, 1984, and 1996, respectively. She worked first as CSIR Senior Research Fellow, then System Development Engineer in a DOE-funded Project in the Department of EE, JU. From 1987, she joined in teaching in the department of EE, JU. She acted as Director of School of Illumination Science, Engineering and Design, JU from 2006 to 2014. She is currently working as a Professor in the Department of EE, JU, Kolkata, India. She has now 33 years of experience in lighting research and teaching. She developed a modernized Illumination Engineering Laboratory in Department of EE, JU. She has founded one full-time Master's Course on illumination engineering and another part-time Master's course on illumination technology and design in JU. She has executed a large number of R&D and Consultancy Projects on illumination and allied fields. Her primary research areas are controllers of lighting systems, renewable energy-based lighting systems, smart lighting systems, LEDs and LASER communication, interior and exterior lighting design, and colour control of modern lighting systems